Characterising the Repetition Rate of CHIME Fast Radio Bursts

I. Simple Models of FRB Repetition

D. Breitman[1,]

McGill University
e-mail: daniela.breitman@mail.mcgill.ca

January 26, 2021

ABSTRACT

The Fast Radio Burst (FRB) population has grown significantly in the past years. In addition to the tremendous growth of the population of one-off FRBs, the Canadian Hydrogen Intensity Mapping Experiment (CHIME) FRB team is also responsible for the discovery of many repeating FRBs. However, CHIME still detects many more one-off FRBs than repeaters. And yet, as the team develops better algorithms to associate new bursts with repeaters, the number of repeats associated with a given repeater is increasing. This development is puzzling: could it be that all FRBs repeat, but not all pulses are being detected? The aim of my thesis is thus to simulate FRB populations starting with a simple model and increase its complexity, to constrain the possibility of all FRBs being repeaters whose burst rate is characterised by the Poisson distribution with a common rate.

1. Introduction

1.1. Fast Radio Bursts

In 2007, Lorimer et al. discover the first fast radio burst (FRB) in archival pulsar data. This pulse was unusual because it seemed to have an extragalacic origin, in contrast to pulsars, which are Galactic objects. Moreover, unlike pulsars, it did not repeat. [Lorimer et al. (2007)]

When a radio pulse is observed, it is dispersed in time because higher frequencies reach the detector before lower frequencies. This delay occurs because lower frequencies move through a plasma of electrons, more slowly than than higher frequencies. Dispersion measure (DM) quantifies this effect: the higher the DM, the more dispersed the signal was, suggesting it crossed a lot of electrons in its path. FRBs are distinguished by the fact that they have unusually high DM in spite of the Milky Way DM contribution to be relatively low. This is why FRBs are thought to be extragalactic.

In 2012, FRB121102 was discovered using the Arecibo telescope PALFA survey [Spitler et al. (2014)]. Follow-up studies later showed that FRB121102 in fact repeats, with the detection of eleven sporadic bursts [Spitler et al. (2016)].

1.2. The Instrument

The Canadian Hydrogen Intensity Mapping Experiment is located in Penticton, BC. Composed of four 20 m by 100 m North-South-oriented cylinders, the telescope was built for cosmology mapping purposes, so it has a very large field of view of about 220 square degrees, and a wide bandwidth from 400 to 800 MHz. CHIME is a transit telescope, and thus has no moving parts. (CHIME/FRB Collaboration 2018)

It turns out that these properties also make CHIME an excellent candidate for FRB detection. Since its first FRB in July 2018, CHIME/FRB detected over 700 FRBs (13 detections published in CHIME Collaboration (2019d)). In addition to single bursts, 18 of these were found to repeat sporadically [CHIME Collaboration (2019a), (2019c)].

Even today, FRBs are still a mystery. Although some emission mechanisms such as Lu and Kumar (2018) and Song et al. (2017) have been proposed, they used the very small sample of FRBs available at the time. As such, there is no general consensus.

These recent detections of FRB sources are of particular scientific value because such an unprecedentedly large sample allows us to statistically confirm or rule out certain assumptions about the nature of FRBs. For example, do all FRBs repeat or are there distinct FRB populations? How are their repeat rates distributed? Answering these questions are the first steps to understanding the emission mechanism and the origin of FRBs.

In this work, we simulate FRB populations and compare them with our data. The hypothesis we consider is that **all FRBs are a single population of repeaters located at cosmological distances whose burst rate is characterised by the Poisson distribution**.

2. Methods

In this section, we describe the simulation process step by step. To run the FRB population simulation, we need four input quantities described in Table 1 below. In this entire section, we will consider $\lambda = 0.6$ bursts/day and $\alpha = -0.1$.

Input Parameters			
Name	Symbol	Unit	Value
Poisson rate	λ	bursts/day	Varies
# FRBs with # bursts > 0	N	repeaters	1000
Power law index	α	—	varies
Luminosity lower bound	L_0	W	10^{32}

Table 1. List of all input parameters and their units in the simulation. We generate FRB populations over different values of α and λ to find the parameters that fit CHIME data best.

In order to generate an FRB population, the simulation requires four input parameters described in Figure 1. The entire simulation process consists of six main parts which we will go over in detail:

1. Generating the FRB population: we randomly generate burst counts following the Poisson distribution for every FRB source.
2. Generating FRB redshifts: we randomly generate redshifts following the constant comoving number density distribution or following the star formation rate. We convert redshifts to distances.
3. Generating FRB sky positions: we generate random FRB positions that are uniformly scattered on the sky. We take scattering of the Milky Way into account since it is less likely to detect an FRB on the Galactic plane.
4. Observing FRBs: we first randomly sample luminosity from a power-law of index α for every burst of every FRB. To convert it to flux, we apply relativistic K-correction. We compare the resulting flux with a flux threshold.
5. Exposure normalisation: we normalise all the simulated bursts with exposure data from CHIME that ranges from August 28, 2018 to July 2, 2019.
6. Comparing with CHIME/FRB data: we normalise CHIME/FRB data over exposure as well and compare it with the simulated data.

2.1. Generating the FRB population

We begin by generating N numbers, each of which corresponds a number of bursts of an FRB. In this work, we suppose that these numbers follow a Poisson distribution.

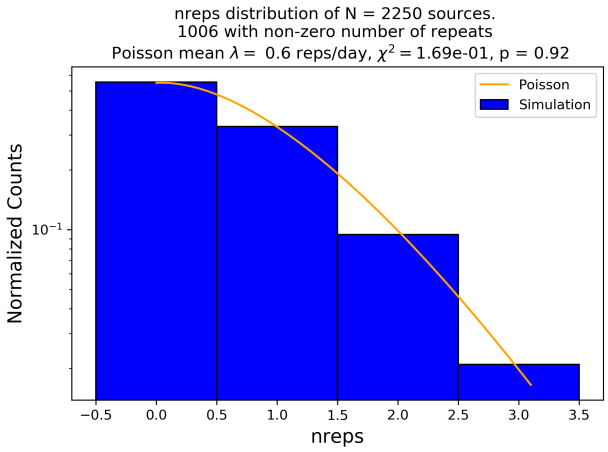

Fig. 1. Histogram of the number of bursts of each simulated FRB source. Note that many do not repeat given the low λ (first bar).

We use the Poisson model with a universal population rate of λ bursts per day:

$$P(k \text{ events}) = \frac{\lambda^k}{k!} e^{-\lambda} \quad (1)$$

To validate this step, we will bin the simulated Poisson numbers, normalise the distribution (blue in Figure 1, and then fit a Poisson distribution (orange in Figure 1 to the bar chart. As expected, we see that they match well, with a high p-value of 0.92.

As seen in Figure 1, it can happen that if λ is small, then many sources don't actually emit any bursts. We keep generating Poisson numbers until we have N FRB sources with at least one burst. For example, in Figure 1, we generated a total of 2250 bursts, until we had 1006 bursts with non-zero repeats. We will truncate this array to 1000 and continue to the next step.

2.2. Generating FRB redshifts and distances

2.2.1. Redshifts

We explore two different redshift models in the simulation process. First, in Figure 2, we consider a constant comoving number density redshift distribution, which corresponds to picking redshifts uniformly in volume. We make no assumptions about the nature of FRBs using this redshift distribution.

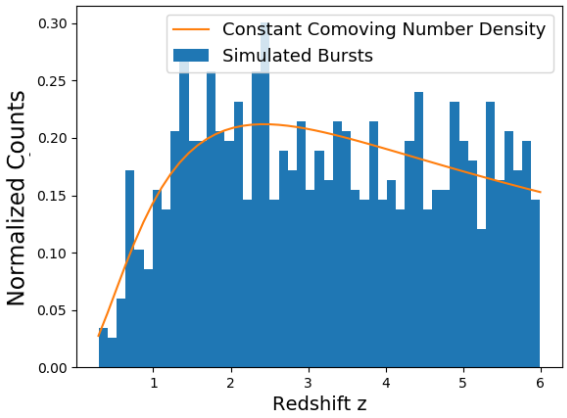

Fig. 2. Distribution of redshifts following a constant comoving number density. Credit to Pragya Chawla for this code.

The second redshift model follows the star formation rate (SFR) as seen in Figure 3. This model is interesting to use if we assume that FRBs are young objects, which has been suggested by some studies such as Munoz (2019). If so, then we would expect FRBs to be located in young galaxies i.e star forming galaxies.

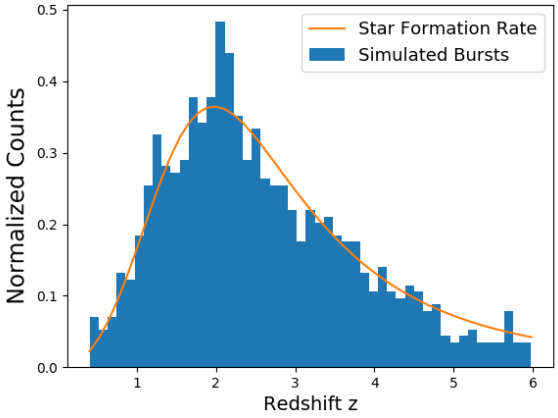

Fig. 3. Distribution of redshifts following the star formation rate (SFR). Credit to Pragya Chawla for this code.

Many thanks to Pragya Chawla for the code to generate both the comoving and SFR redshift distributions in the two figures above.

2.2.2. Luminosity distance

Using the redshift z, and the Planck 15 cosmology[ref planck 2015 paper 13], we calculate the luminosity distance of every FRB to Earth, d_L, using: [planck 15]

$$d_L = (1 + z) \cdot D_M, \tag{2}$$

where D_M is the transverse comoving distance.

In Figures 4 and 5, we see the luminosity distance distribution resulting from the redshifts following comoving number density and SFR, respectively.

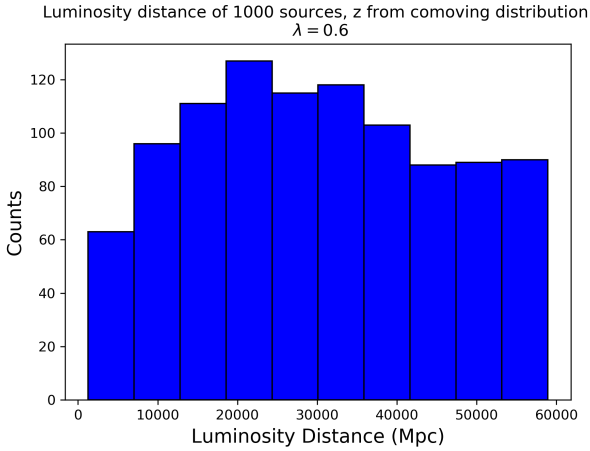

Fig. 4. Distribution of luminosity distances calculated using the comoving redshift distribution in Figure 2 and Equation 2.

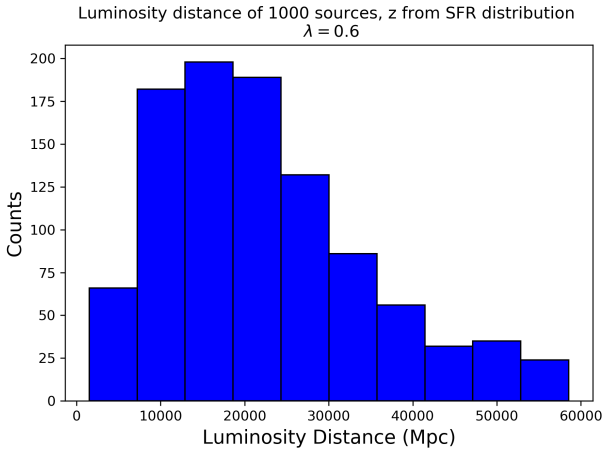

Fig. 5. Distribution of luminosity distances calculated using the SFR redshift distribution in Figure 3 and Equation 2.

2.3. Generating FRB positions

We first generate FRBs positions uniformly on the sky, by sampling a right ascension (RA) and declination (Dec) as seen in Figure 6.

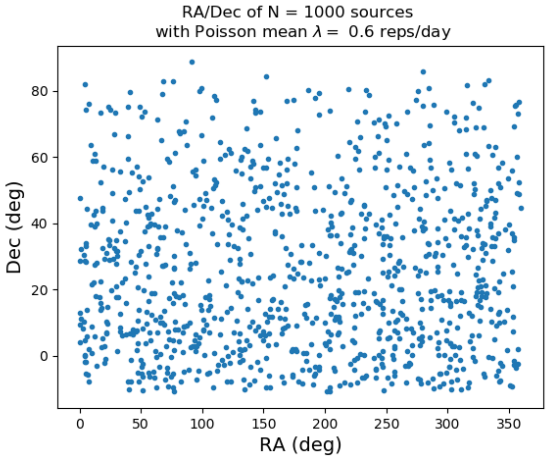

Fig. 6. Declination as a function of right ascension for N = 1000 uniformly distributed sources on the sky.

2.3.1. Scattering Timescale

CHIME searches for pulses up to observed pulse widths of 63 ms [Z. Pleunis]. We will consider sources with a higher scattering time (aka pulse broadening) than 63 ms as undetectable.

To estimate scattering timescale due to the Milky Way, we use the PyGEDM package which provides a Python interface with the commonly-used free electron density model NE2001.[Cordes, Lazio (2003)]

We fix a distance at the edge of the galaxy: $D = 30$ kpc and calculate the scattering times at this distance for lines of sight along the RA and Dec of every simulated FRB using the NE2001 model.

For a given line of sight, PyGEDM returns the scattering measure for pulse broadening (SM_τ):[Cordes, Lazio (2003)]

$$\mathrm{SM}_\tau = 6 \int_0^D ds \;\; (s/D) \cdot (1 - s/D) \cdot C_n^2, \tag{3}$$

where C_n is calculated by the model and depends on the line of sight. We can then calculate the scattering time in ms using:[Cordes, Lazio (2003)]

$$\tau_d = 1.10 \cdot \mathrm{SM}_\tau^{6/5} \nu^{-22/5} D, \tag{4}$$

where $\nu = 0.600 GHz$ for CHIME.

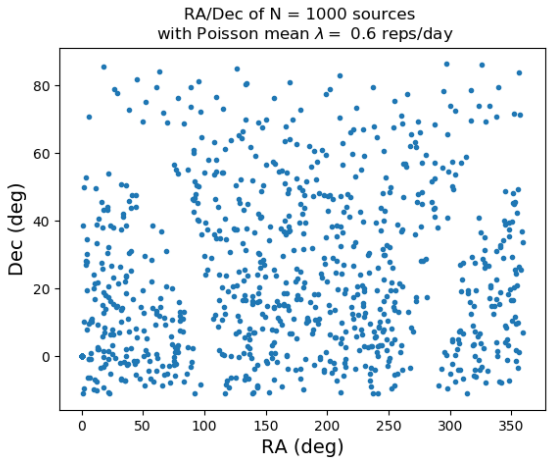

Fig. 7. Declination vs right ascension for N = 1000 uniformly distributed sources on the sky after eliminating locations whose lines of sight have scattering timescales higher than 63 ms. The emptiness in the plot traces the Galactic plane as expected.

Figure 7 shows the RA vs Dec plot after the FRB locations with Galactic scattering larger than 63 ms have been eliminated. As expected the eliminated sources form a cut arc in the plot which corresponds to the Galactic plane.

Note that this is not the ideal method to estimate the Galactic contribution to pulse scattering for extragalactic pulses. After some discussion with the authors of the model NE2001 James Cordes and Joseph Lazio, a more appropriate method has been found. However, for now it involves working with the FORTRAN code of NE2001, so this improved solution will be implemented in future work.

Also note that it is possible to estimate a pulse scattering time due to the host galaxy of the FRB. This was omitted in this work, but will be implemented in future work.

Lastly, it is important to mention that in this step as well we want a final number of N RA, Dec pairs. If at a first pass, many RA,Dec pairs have been eliminated, we keep generating more until we have N (RA, Dec) pairs with scattering under the threshold.

2.4. Generating flux measured at CHIME

At this stage, we have N sources, each of which emitted some number of bursts chosen from a Poisson distribution of mean λ over an exposure time. The next step is to evaluate how many of these can be detected at CHIME.

To do so, we must randomly pick a luminosity for each burst. Luminosity is the amount of light emitted by an object per unit time i.e. in W. It is independent of an observer's distance from an object. Luminosity is then converted to flux, which is the distance-dependent quantity that allows us to distinguish detectable bursts from undetectable ones.

2.4.1. Luminosity

In this work, we assume that luminosity follows a power-law distribution with index α. The luminosity function $N(L)$ is the density of FRBs as a function of their bolometric luminosity L in W:

$$N(L) = \phi^* L^\alpha, \tag{5}$$

where $\phi*$ is a normalisation factor, and α is the power law index. We find the normalisation constant ϕ^* by integrating the power law:

$$\int_{L_0}^{L_1} \phi^* L^\alpha = \phi^* \frac{L^{\alpha+1}}{\alpha+1}\Big|_{L_0}^{L_1} = 1$$
$$\implies \phi^* = \frac{\alpha+1}{L_1^{\alpha+1} - L_0^{\alpha+1}}$$

This implies that $\alpha \neq -1$ and that we must define a lower bound for the luminosity. In our simulations, we attribute a randomly generated luminosity to each source according to Equation 5. Given a uniform random variable $y \in [0, 1]$, we calculate a power law distributed random variable R in the following way:

$$y = \int_{L_0}^{R} \phi^* L^\alpha = \phi^* \frac{R^{\alpha+1} - L_0^{\alpha+1}}{\alpha+1}$$
$$\implies R = \left(\frac{y(\alpha+1)}{\phi^*} + L_0^{\alpha+1}\right)^{1/(\alpha+1)}$$

If we let $L_1 \to \infty$:

$$R = L_0 \cdot (1-y)^{\frac{1}{\alpha+1}} \tag{6}$$

In Figure 8, we see the resulting distribution of N = 1000 random power-law generated luminosities according to Equation 6.

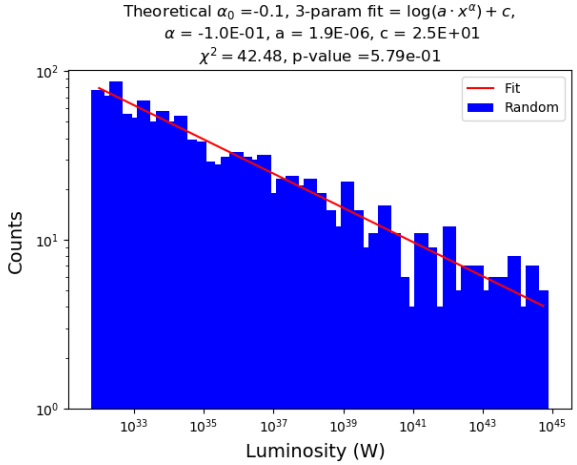

Fig. 8. Distribution of randomly generated luminosities with a power-law fit.

2.4.2. K-Correction

The next step is to calculate the flux density. However, we will not simply use: [Ryden (2016)]

$$F = \frac{L/\Delta\nu}{4\pi d_L^2 (1+z)^2} \tag{7}$$

As a sanity check, Figure 9 shows the flux distribution without K-correction.

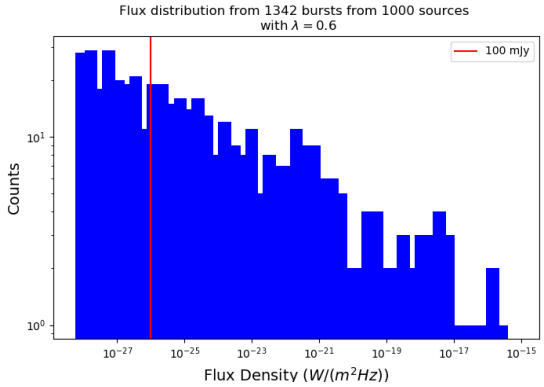

Fig. 9. Flux distribution without K-correction using Equation 7.

Instead, we will correct for the fact that the observed frequencies (400 - 800 MHz) have been redshifted so we observe a portion of the FRB spectrum produced at different frequencies (ν_l - ν_h MHz), which depend on the source redshift.

For a source at redshift z, we have that the emitted frequency ν_e and the observed frequency ν_o are related by: [Hogg, Baldry, et al. (2002)]

$$\nu_e = (1+z)\nu_o \tag{8}$$

We calculate the total flux density over the observation bandwidth using Equation 9 in [Lorimer, Karastergiou, et al. (2013)]:

$$S = \frac{L}{4\pi(1+z)d_L^2} \cdot \frac{1}{f_h^{\alpha+1} - f_l^{\alpha+1}} \cdot \frac{\nu_h^{\alpha+1} - \nu_l^{\alpha+1}}{\nu_h - \nu_l}, \tag{9}$$

where L is luminosity in erg/s, d_L is luminosity distance in cm, z is redshift, $f_l = (1+z)\cdot 400$ MHz, $f_h = (1+z)\cdot 800$ MHz. As in Lorimer, Karastergiou, et al. (2013), we assume that FRBs emits over a very large frequency range. However, we take $\nu_l = 200$ MHz, since the lowest frequency at which FRBs are currently known to emit is 300 MHz [P Chawla et al. (2020)] . We take $\nu_h = 8$ GHz, since Gajjar, Siemion, et al. (2018) found that FRB121102 emits at such high frequencies. Following Lorimer, Karastergiou, et al. (2013), we take energy power law index $\alpha = -1.4$.

Figure 10 shows the resulting flux density distribution, where the red line is at 200 mJy, which we consider as our smallest cutoff. We take 200 mJy as the flux lower bound since in CHIME Collaboration (2019b), the faintest reported burst is around 300 mJy.

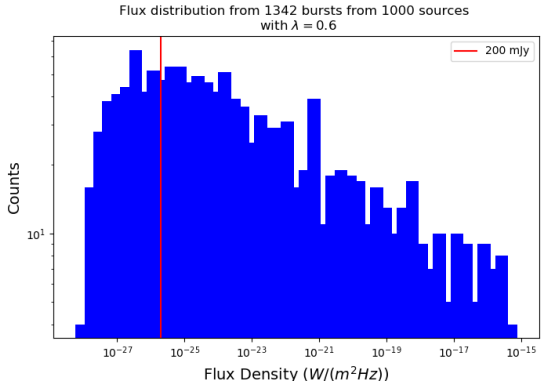

Fig. 10. Distribution of fluxes after K-correction has been applied. We reject at least all sources to the left of the red line as we consider them too faint. Note that this process eliminates approximately 20 % of the N simulated FRBs.

Upon comparing Figures 9 and 10, we see that the orders of magnitude of the flux values are roughly the same, but the distribution is different. The K-corrected flux distribution has very few bursts at the low flux end, unlike the classical flux distribution.

CHIME has different sensitivity for different parts of the sky, like a beam of a circular dish is more sensitive to signals at its centre than on its edges. Due to its unique design, CHIME has a very complex sensitivity pattern. However, in this work, we will only take into account its primary beam structure i.e the sensitivity along each of the four cylinders is best at the centre of the cylinder rather than at the top/bottom as seen in Figure 11.

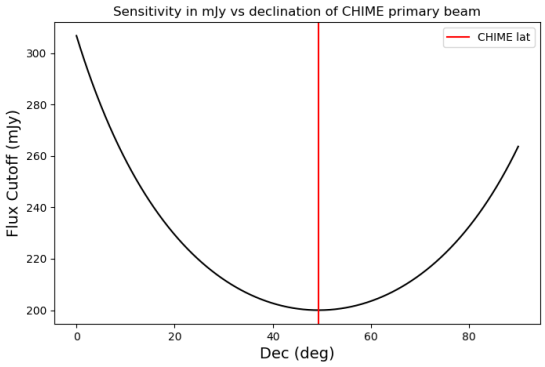

Fig. 11. We vary the flux cutoff as a function of declination to account for the CHIME primary beam. The red line corresponds to zenith. It is also where the flux cutoff is lowest and is consequently the most sensitive area of the primary beam.

After calculating the flux, we reject all bursts with flux density under the flux threshold. From Figure 10 above, we see that this implies in rejecting at least 20 % of the simulated FRBs. In Figure 12, we show the distribution of the number of repeats of every FRB. Note that most sources only repeat once.

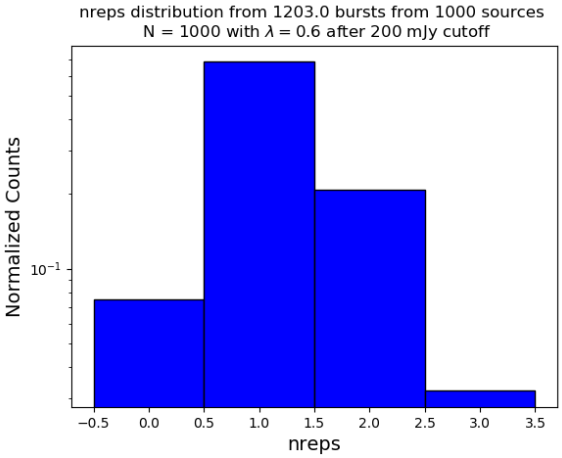

Fig. 12. Distribution of the number of bursts per FRB after applying the flux cut.

2.5. Normalisation

The last step is to normalise the simulation data by exposure and primary beam sensitivity so that it is comparable with the data.

2.5.1. Exposure

We observe more FRBs from certain regions on the sky because the telescope sees them for longer periods of time. The rotation of the Earth and the position of the telescope determine how long a patch of sky is visible to us. Due to the location of the telescope in the northern hemisphere, in general, we see patches of sky at higher declinations for longer meaning they have higher exposure. We may have missed a lot of bursts from the source at the lower declination merely due to its location. Exposure acts as a normalising factor. Recall that CHIME is a transit telescope, so on average, we observe a patch of sky for about 6 minutes/day.

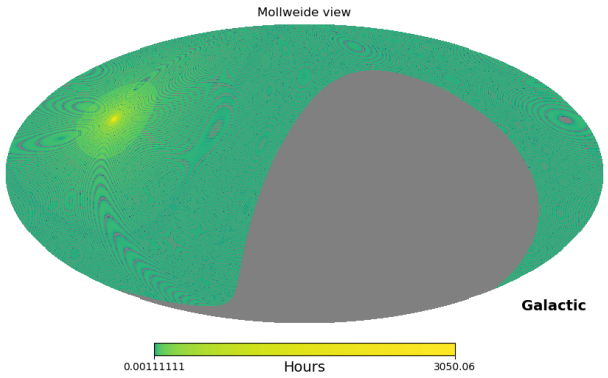

Fig. 13. CHIME exposure map up to July 2, 2019 with both upper and lower transits. Credit to Pragya Chawla for the data. The brightest yellow spot is the North pole which the telescope sees at all times.

The exposure map used in this simulation is shown in Figure 13. This exposure map includes both the exposure due to the lower and the upper transits from August 28, 2018 until July 2, 2019. The lower transit is the additional yellow circular patch centered around the bright yellow dot of the North pole. It corresponds to the fact that we observe a range of high declinations 'on the other side' of the north pole (hence the term 'lower' transit). However, we must note that this map is incomplete in the sense that some locations have zero exposure as can be seen in the little grey arcs on the map. In this work, whenever an FRB with at least one burst is observed in that region, we ignore it. Currently this involves ignoring approximately 5% of the N simulated FRBs.

Recall that in this work, we consider data and exposure from August 28, 2018 up to July 2, 2019. To fix the lack of exposure data, we can simply consider more data i.e. use CHIME data and exposure map data until a later date.

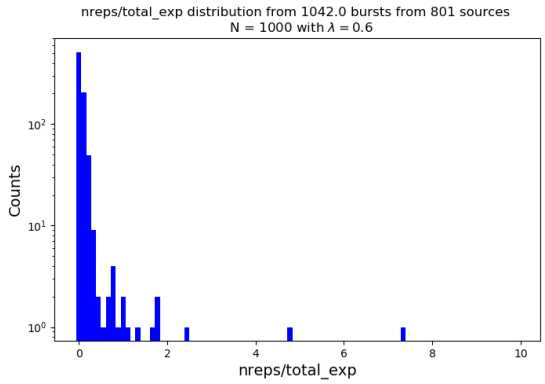

Fig. 14. Distribution of the number of repeats per FRB after normalising by exposure only. Notice that we only have 805 sources with more than one repeat left after applying the flux cutoff.

Together with the flux cutoff, this implies that for a given run of the simulation, we end up rejecting approximately 20 % of the N simulated FRBs. For example, in all of the above figures, we worked with N = 1000. This elimination explains why the final number of simulated FRBs in Figure 14 is 801.

2.6. CHIME Data

In this work, we compare our simulations to CHIME/FRB data from August 28, 2018 up to and including July 2, 2019. This includes 17 repeaters and 502 one-off FRBs as can be seen in Figure 15.

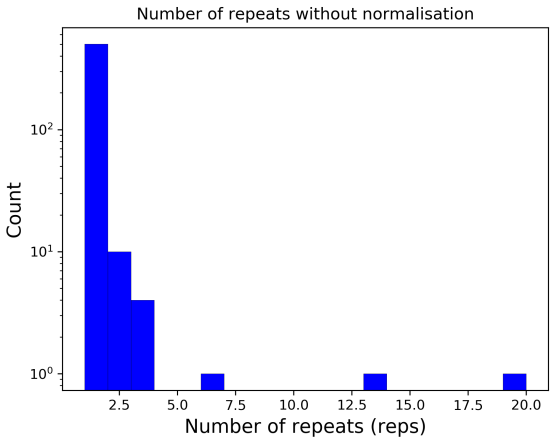

Fig. 15. CHIME/FRB data from August 28, 2018 up to and including July 2, 2019. There are 502 single bursts and 17 repeaters. They are not normalised.

Like for the simulated FRBs, we normalise the data by telescope sensitivity and exposure. The result of this normalisation is shown in Figure 16.

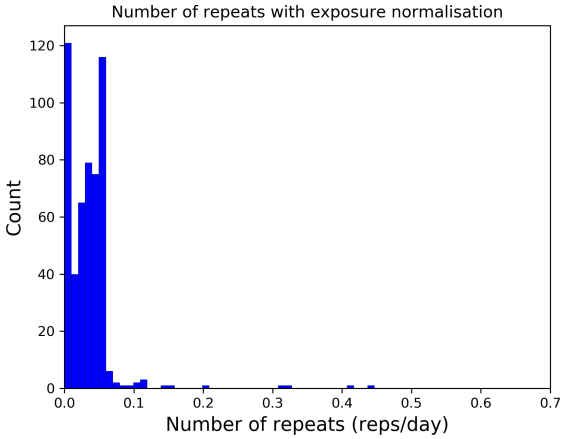

Fig. 16. Figure 15 normalised over exposure. Number of sources that have a given number of repetitions per exposure. There are 502 single bursts and 17 repeaters, each normalised by the exposure according to its RA and Declination.

The final step is to compare the results of the simulation with the data. We bin both the data and the simulation results in 70 bins to compare them as seen in Figure 17 below.

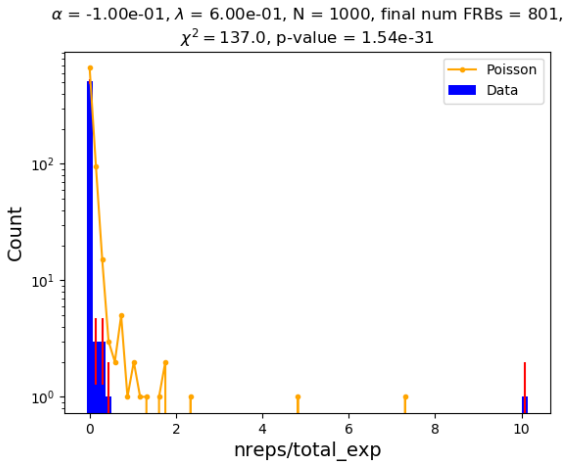

Fig. 17. Comparison of CHIME/FRB data up to July 2, 2019 and simulated data. CHIME/FRB data consists of a total of 519 sources, while the simulation yielded 801 FRB sources.

Although the first bins are almost identical in the data and the simulation, the later bins fall off much faster in the data than in the simulation, hence the high χ^2.

In the following section, we explore the parameter space of the simulation when fitting various values of luminosity index α and Poisson rate λ. We will also discuss consequences of varying the number of simulated FRBs N.

3. Results

We can use the simulation results to prove or disprove the hypothesis that FRBs are **a single FRB population of repeaters governed by a common Poisson mean**.

After developing a method to simulate FRB populations, our goal is to find the set of parameters (N, α, λ) that fit the data best. This task can be approached in two ways: brute force searching through parameter space (very expensive computationally), or ad hoc parameter guessing before exploring a much smaller parameter space (much less expensive computationally).

3.1. Parameter Space

In this subsection, we attempt the first method mentioned. We run the simulation over multiple (N, α, λ) triples, repeating it ten times for every set of values. We record the minimum, average, and maximum χ^2 over the ten iterations for every set of parameters.

Since this computation is very expensive, only a small range of parameter values with large gaps has been explored in this work, and is shown in Figures 18, 19, and 20.

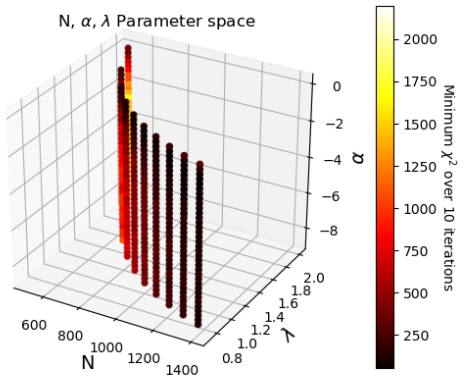

Fig. 18. A small parameter region. The colour bar represents the minimum χ^2 after 10 iterations of the parameter set.

The curves in these plots are due to the method used to choose the N and λ parameters, which is $N \cdot \lambda$ = constant. This method was important in earlier stages of development to keep the number of simulated FRBs roughly the same as the number of CHIME/FRB data sources. They do not represent any real dependence of the parameters.

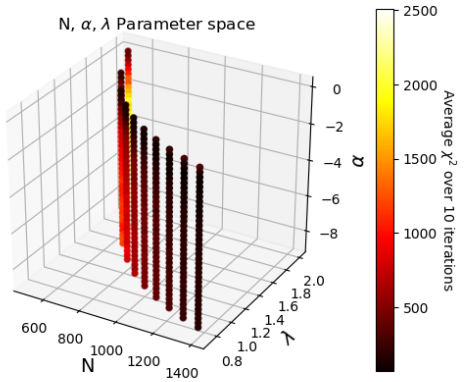

Fig. 19. A small parameter region. The colour bar represents the average χ^2 after 10 iterations of the parameter set.

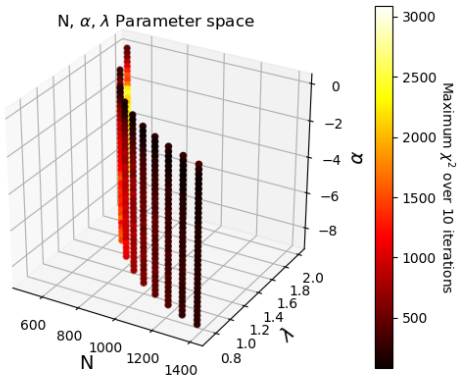

Fig. 20. A small parameter region. The colour bar represents the average χ^2 after 10 iterations of the parameter set.

As a whole, we can see that the χ^2 varies as a function of α. This fact is very difficult to see in individual plots such as the ones in the next section.

3.2. Correlation

The parameters N, α, λ are correlated i.e. each one does not control an independent aspect of the simulation. Consequently, it's more difficult to explore the parameter space in the quest of finding the best fit. For example, in Figures 21 - 23 below, we can see three very similar simulation results, but with wildly different parameter values for each.

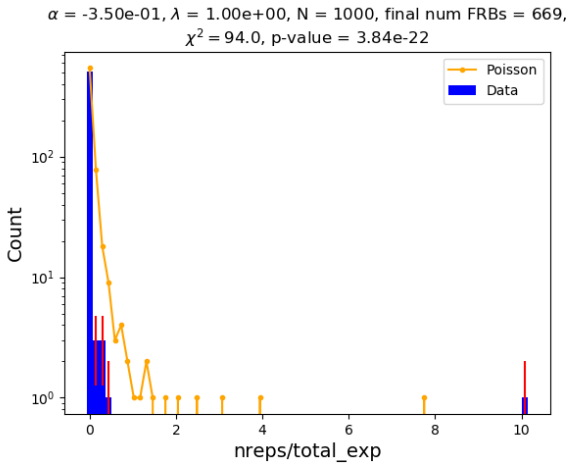

Fig. 21. Comparison of CHIME/FRB data with simulation results. Note that this is only one instance of the simulation, and thus running these same parameters many times will produce different outcomes.

In Figure 21 above, we have N = 1000, $\alpha = -0.1$, and $\lambda = 0.6$ reps/day. In comparison, in Figure 22, we have very different parameters: N = 3000, $\alpha = -1.00 \cdot 10^{10}$, $\lambda = 9.00 \cdot 10^{-6}$ reps/day. Of course, such a value for α is not physical. This is just to show how very different parameters can yield similar results. Nonetheless, Figure 22 being a better fit indicates that a higher N with a lower λ might describe the data better.

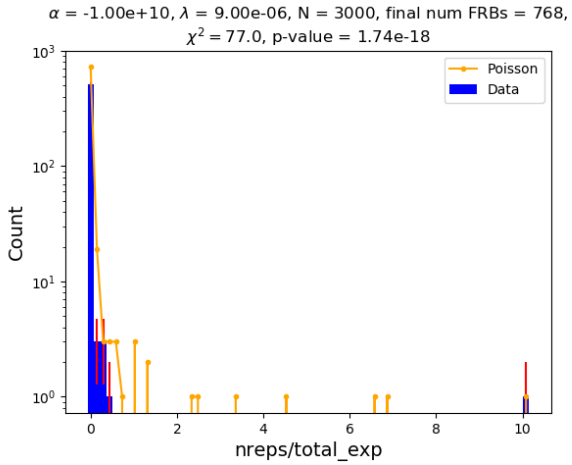

Fig. 22. Comparison of CHIME/FRB data with simulation results. Note that this is only one instance of the simulation, and thus running these same parameters many times will produce different outcomes. Also note that this value of α is not physical. We compare this to the previous figure.

In Figure 23, we decrease N to 2000 and λ to $1 \cdot 10^{-6}$. We change α to -2.0 (orders of magnitude in difference in comparison to the two other Figures), and yet again the result is very similar to the two other figures. The parameter α is responsible for the sharpness of the slope in Figure 8. A very low α as in Figure 22 implies that the luminosity values will be very close to the minimum luminosity L_0. On the other hand a higher α as in Figure 8 allows for a bigger range of luminosities.

Recall that the Figures in the previous subsection, such as Figure 18, confirm that χ^2 does change smoothly for different values of α while N and λ are fixed.

We can conclude the index value of the luminosity power law affects the flux in a very subtle way that is worth further study. This also suggests that perhaps the luminosity lower bound L_0 that we are currently using (see Table 1) is too large and may require some tweaking.

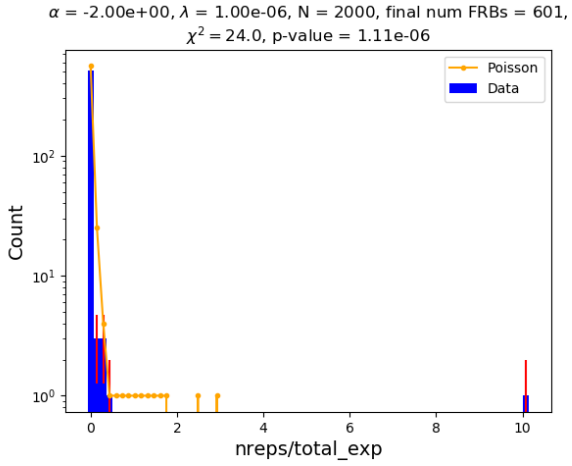

Fig. 23. Comparison of CHIME/FRB data with simulation results. Note that this is only one instance of the simulation, and thus running these same parameters many times will produce different outcomes.

4. Conclusion

In this work, we develop a method to simulate FRB populations at cosmological distances with burst rates characterised by the

Poisson distribution. We took into account many important effects such as scattering due to the Milky Way, K-correction, telescope sensitivity, and exposure in our calculations. We've laid a solid foundation for more work to be continued. Moreover, there are many more important biases and factors that have been omitted in this work. For example, we did not take high DM bias into account i.e. it is more difficult to detect bursts with very high DMs. Another example is pulse width. It is known that the detection threshold of CHIME changes depending on pulse width. However, this is not yet quantified. Finally, repeaters tend to have wider pulses, and by the previous remark, CHIME may have a bias against detecting repeaters vs one-off FRBs. All of these effects have not yet been quantified, but could significantly change the simulation outcomes.

Acknowledgements. Many thanks to my supervisor, Victoria Kaspi. The project was part of the Repetition Working Group. The RWG would host a telecon every two weeks where I'd share my updates and members of the group, such as Paul Scholz, Shriharsh Tendulkar, and Pragya Chawla, would give feedback and suggestions that helped me a lot in advancing in my work.

References

CHIME Collaboration. 2019a, ApJL, volume 885
CHIME Collaboration. 2019b, ApJ, volume 885, id. L24, pp. 26
CHIME Collaboration. 2019c, ApJL, volume 891
CHIME Collaboration. 2019d, Nature, volume 566, pp. 230
CHIME/FRB Collaboration. 2018 [ArXiv 1803.11235]
Cordes, Lazio. 2003 [arXiv:astro-ph/0207156v3]
Gajjar, Siemion, et al. 2018, ApJ, volume 863, id. 2, pp. 9
Hogg, Baldry, et al. 2002 [arXiv:astro-ph/0210394]
Lorimer et al. 2007, Science, volume 318, pp. 777
Lorimer, Karastergiou, et al. 2013, MNRAS, volume 436, pp. L5
Lu and Kumar. 2018, MNRAS, volume 477, pp.2470
Munoz. 2019, ApJ, volume 890, id. 162
P Chawla et al. 2020, ApJL [arXiv:2004.02862]
Ryden. 2016, Introduction to Cosmology (Cambridge University Press)
Song et al. 2017 [arXiv:1707.08979]
Spitler et al. 2014, ApJ, volume 790, pp. 9
Spitler et al. 2016, Nature, volume 531, pp. 202